2nd URSI AT-RASC, Gran Canaria, 28 May – 1 June 2018

Spectral Characterization of Equatorial Plasma Bubbles from High-Resolution Simulations

Charles L. Rino*(1), Tatsuhiro Yokoyama(2), and Charles S. Carrano(1)
(1) Institute for Scientific Research, Boston College, USA
(2) National Institute of Information and Communications Technology, Koganei, Tokyo, Japan

Abstract

Manifestations of severe nighttime equatorial ionospheric disturbances have been observed for decades. It is generally accepted that the phenomena are caused by large depletions, referred to as equatorial plasma bubbles (EPBs), which are initiated on the rising unstable bottom side of the nighttime F layer. Physics-based simulations have enhanced our understanding of the EPB phenomenon. However, until very recently stochastic structure smaller than ~ 10 km was unresolved. More recent high-resolution EPB simulations have extended the resolution to hundreds of meters. These new results have provided a unique opportunity to characterize evolving height-dependent EPB structure.

This paper presents a summary analysis of time-space EPB structure evolution. A wavelet-based structure classification procedure identifies developed structure and estimates parameters that define a two-component inverse-power-law spectral density function.

1 Introduction

High-resolution simulations as described in the survey paper by Yokoyama [Yok17] were made available for the EPB structure analysis. Figure 1, which is taken from [Yok17], shows a perspective view of an EPB configuration at 3600 seconds. The structure development involves magnetic-field-aligned flux tubes that terminate at low altitudes in opposite hemispheres. One-dimensional spectral density functions (SDFs) separately averaged cross-field and along the vertical dimension provide an overall characterization of the structure. Figure 1 in Yokoyama [Yok17] shows averaged cross-field and vertical one-dimensional spectral density functions (SDFs) from the equatorial plane realization at 3600 s. Both SDFs follow inverse two-component power laws with a break at the spatial frequency corresponding to structure between 1 and 10 km.

Figure 2 shows the structure in the equatorial plane at 3600 sec. A wavelet-based analysis procedure was developed to identify the zonal structure at each altitude that could be represented by a one-dimensional spectral density function (SDF) of the form

$$\Phi_{N_e}(q_y) = C_s \begin{cases} q^{-\eta_1} & \text{for } q \le q_0 \\ q_0^{\eta_2-\eta_1} q^{-\eta_2} & \text{for } q > q_0 \end{cases} . \qquad (1)$$

The hypothesis is accepted if the parameters C_s, η_1, q_0, and η_2, can be adjusted to reduce a goodness-of-fit measure below a predetermined threshold. The analysis was applied to equatorial plane structure and two offset planes as shown in Figure 3

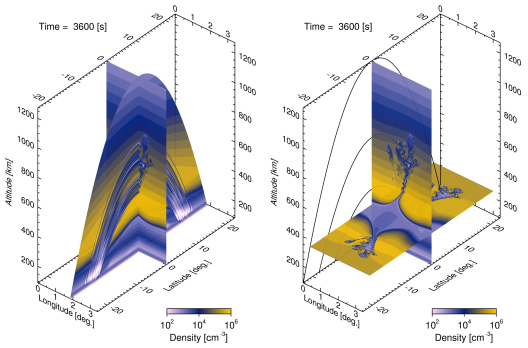

Figure 1. Perspective view of the EPB simulation environment. The left frame shows the central meridian plane. The right-hand frame shows the structure in two orthogonal slice planes.

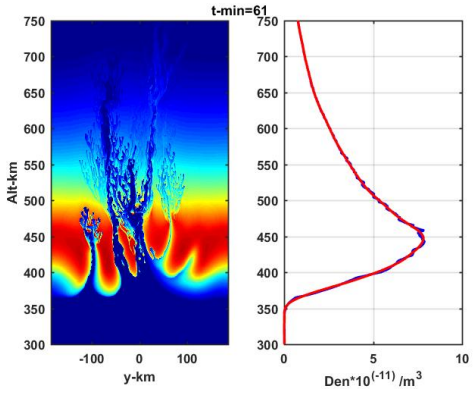

Figure 2. The left hand frame shows the equatorial plane structure at 3600 s. The right-hand frame is the path-integrated density (blue) with a smoothed profile overlaid.

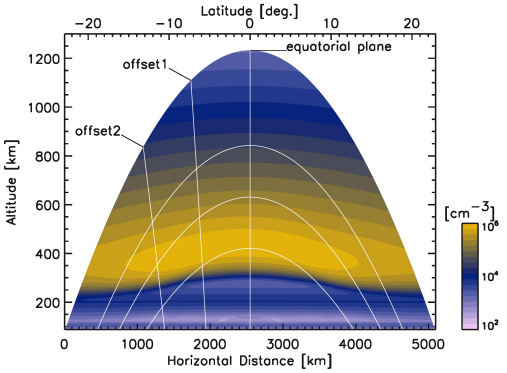

Figure 3. Meriodinal slice plane with overlaid rays locating vertical equatoral slice plane and two offset slice planes, denoted offset 1 and offset 1, excised for structure analysis.

2 Results

Figure 4 is a scatter diagram of C_sdB versus η_1 and η_2 Irrespective of where or when developed structure is captured, the C_sdB versus η_1 estimates follow the log-linear relation

$$\eta_1 = -\eta_0(C_sdB - C_0dB), \qquad (2)$$

with $\eta_0 = 0.02$ nepers per dB. The red lines in Figure 10 are derived from (2) with $C_0dB = 240$ dB. For $C_sdB > C_0dB$ both the model and observed η_1 values are negative, which implies that large-scale structure is being suppressed rather than enhanced.

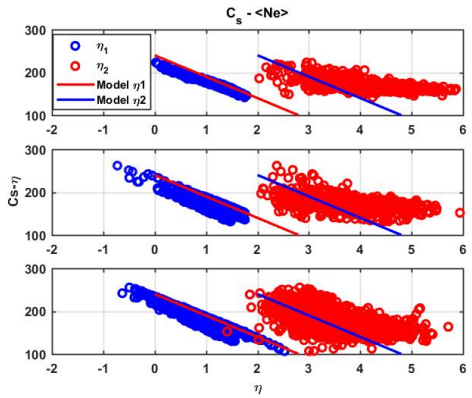

Figure 4. Scatter plots of C_sdB versus η_1 (blue circles) and η_2 (red circles). Lower frame is Equatorial. Middle frame is offset 1. Upper frame is offse2. The solid red lines are derived from 2. The solid blue lines are offset by 2.

Figure 5 shows scatter diagrams of C_sdB versus $\log 10(q_0/(2\pi))$. For $2\pi/q_0 > 10$ km, there is decrease in $\log 10(q_0/(2\pi))$ with increasing C_sdB similar to the η_1 dependence. Upon inspection of the SDFs with break sales approaching $log10(q_0/(2\pi)) = -4.5$, it was found, similarly, that the SDFs are well represented by the model. SDFs with a negative large-scale index or a large break scale ($(2\pi)/q_0 > 30$ km) can be associated with initiating structure following the onset of bifurcation.

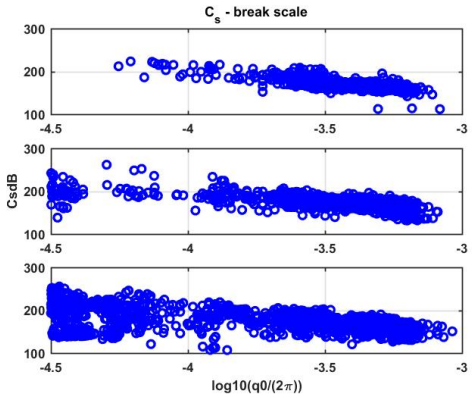

Figure 5. scatter plots of C_sdB versus $log10(q_0/(2\pi))$. Lower frame is equatorial. Middle frame is offset1. Upper frame is offset2.

The range $0 < \eta_1 < 3$ is representative of two-component inverse-power-law SDFs. The associated η_2 values are larger but more variable. As a visual guide, the blue lines in Figure 4 are offset by 2 units from the η_1 values. However, there is a point were extrapolated index values become too large. In the offset 1 and offset 2 data all the C_sdB values are greater than 130 dB. In the equator data as η_1 values for small C_sdB approach 2, the associated η_2 and break-scale values are scattered such that a single power-law extension of (2)provides a good fit. This small population is the only EPB structures that can be characterized by a single inverse-power-law SDF.

3 Discussion

Overall, developed EPB structure is characterized by two-component inverse-power-law SDFs. The log-linear relation (2) is the defining relation irrespective of time after onset or where the structure is intercepted in the EPB data space. No negative η_1 values were found in the offset 2 data, which only sampled structure above the F-region peak. The subset of two-component power-law SDFs that have negative power-law index values are incorporated as a special category. Figure 6 shows SDF examples of the three spectral types.

The relation between the large-scale power-law index and the turbulent strength was observed in the PLUMEX data as reported in Rino et. al [Rin81]. The relation had been inferred earlier from analysis of Wideband Satellite beacon data. The PLUMEX paper Equation 1 was taken from Livingston et. al [Liv81]. The PLUMEX paper Figure 7 shows the relation from SDFs derived at two different altitudes. It should also be noted that the significant vertical motion of the PLUMEX rocket supports the hypothesis that EPB cross-field structure is isotropic. The EPB structure classification is in nearly complete agreement with the measured PLUMEX characteristics.

These spectral characteristics appear to be intrinsic to the

convective instability process. Evidently, increasing large-scale structure intensity is constrained in a way that causes a decrease in the spectral index and a decrease in the scale range over which the structure increase is developing.

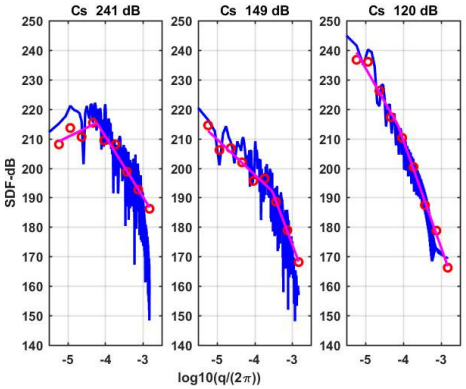

Figure 6. Examples of EPB SDF types. Left frame: outer scale. Center frame: two-component. Right frame: single component.

4 Acknowledgements

This work was supported by JSPS KAKENHI Grant Number JP16K17814. This work was also supported by the computational joint research program of the Institute for Space-Earth Environmental Research (ISEE), Nagoya University, Japan.

Support for CR and CC was provided under Advanced Data Driven Specification and Forecast Models for the Ionosphere-Thermosphere System, Air Force Contract FA9453-12-C-0205

References

[Liv81] Livingston, R.C, Rino, C.L, McClure, J.P, Hanson, W.B (1981) Spectral characteristics of medium-scale equatorial f-region irregularities. J. Geophys. Res 86, 7421–7428

[Rin81] Rino, C.L, Tsunoda, R.T, Petriceks, Livingston, R.C, Kelley, M.C, Baker, D K (1981) Simultaneous rocket-borne beacon and in situ measurements of equatorial spread f–intermediate wavelength results. J. Geophys. Res 84(A4), 2411–2420

[Yok17] Yokoyama, T (2017) A review on the numerical simulation of equatorial plasma bubbles toward scintillation evaluation and forecasting. Prog. Earth Planet. Sci., **4:37**(doi:10.1186/s40645-017-0153-6, 2017)